

Hadron Deformation and Form Factors from Lattice QCD

C. Alexandrou

Department of Physics, University of Cyprus, CY-1678 Nicosia, Cyprus

Abstract. We review the current status of lattice QCD studies of the nucleon system. In particular, we focus on the determination of the shape of the nucleon by probing its wave function as well as by evaluating the N to Δ transition form factors.

I. INTRODUCTION

Lattice QCD provides an indispensable method in our efforts to solve Quantum Chromodynamics (QCD). It is the only approach, using directly the QCD Lagrangian, available up to now in the energy regime between high energy processes, where perturbation theory is applicable, and very low energies, where chiral perturbation theory can be used. Lattice QCD is a discretized version of QCD formulated in terms of path integrals on a space-time lattice [1] with only parameters the bare quark masses and the coupling constant, like the continuum theory. One recovers continuum physics by extrapolating results obtained at finite lattice spacing a to $a = 0$. In order to perform the continuum extrapolation a separate calculation at several values of a is required. Because this can require large computer resources, in most cases, the strategy is to work close to the continuum limit, either by choosing a sufficiently small or by improving the discretization scheme to eliminate order- a terms. Numerical evaluation of observables in lattice QCD necessarily requires that the size of the lattice is finite. To keep the size of the box large enough to fit the hadrons well inside one must increase the number of sites as one decreases a . Therefore calculations at decreasing values of a require increasingly larger computer resources. To keep finite volume effects small one must have a box that is much larger than the Compton wavelength of the pion. Usually we take $Lm_\pi \gtrsim 5$ where L is the spatial length of the box and m_π the pion mass. In an actual calculation the bare quark masses for the u and d quarks are taken larger than in the real world. Given that computational costs increase like m_π^{-9} , the use of larger quark masses enables inversion of the fermionic matrix, needed for the calculation of hadronic matrix elements, with currently available resources. To extract physical quantities from lattice calculations typically done with pion masses above 350 MeV, one needs to extrapolate to the physical quark masses. It is only very recently that we can reliably reach pion masses, below 350 MeV [2, 3]. This is a very important step forward in our effort to eliminate one source of systematic error associated with the extrapolation to the light quark masses. Typical state-of-the art lattices use $a \lesssim 0.1$ fm and $L \sim 3$ fm for pions of mass down to about 350 MeV.

Discretization of space-time introduces an ultra-violet cut-off limiting the highest momentum to $2\pi/a$. Therefore, the lattice provides a regularization of the ultra-violet divergences of the theory making it well defined from the start. Working in a finite box allows only discrete values of momentum in units of $2\pi/L$. The bare coupling constant and quark masses are tuned as a changes to leave physical quantities unchanged. Besides using a finite lattice spacing, a finite volume and heavier u - and d - quarks, an additional step, that enables us to numerically evaluate the path integrals needed, is rotation to imaginary time, $t \rightarrow -it$, resulting in replacing $\exp(iS)$ by $\exp(-S_E)$ where S (S_E) is the classical QCD action in Minkowski (Euclidean) space. Having a real action one can apply stochastic methods commonly used in statistical mechanics to evaluate the path integrals. Whereas finite a , volume and quark masses are amenable to systematic improvements, rotation to Euclidean space selects a set of observables that can be studied within this framework. These are observables that can be determined from the properties of the discrete lower lying states. For this set of observables, lattice QCD produces the exact answer provided the extrapolations to the continuum and infinite volume limits as well as to the physical quark masses are under control.

In a typical lattice calculation one starts by choosing the bare coupling constant g , which fixes the lattice spacing, and the bare masses for the u -, d - and s -quarks. One then computes a physical quantity such as the mass of the pion

and the nucleon in lattice units as a function of the quark mass. The pion mass is used to fix the u- and d- quark masses (assumed degenerate) and the mass of the kaon or ϕ to fix the strange quark mass whereas the lattice spacing is determined by extrapolating the results, for instance, for the nucleon mass to the physical pion mass. Any other physical quantity in the light quark sector then follows. If instead of the nucleon mass one chooses another physical quantity such as the pion decay constant, f_π , to set a the resulting value should be the same if finite lattice volume and non-zero a effects are under control.

Like in the continuum, the lattice QCD action, $S_E = S_g[U] + S_F[U, \bar{\psi}, \psi]$, has a purely gluonic part S_g written in terms of the gauge link $U_\mu(n) = \exp(iagA_\mu(n))$, which connects site n with $n+1$ in the μ -direction and a fermionic part S_F , which contains the kinetic energy of the quarks and the interaction terms. $A_\mu(n)$ denotes the gluon field. Gauge symmetry is exactly preserved by S_E . As in any renormalizable theory, the fermionic action is bilinear in the fermion fields and can be written in terms of the fermionic matrix D as $S_F = \sum_{n,j} \bar{\psi}(n) D_{nj} \psi(j)$. The exact form of D depends on the discretization scheme used for the fermions. The simplest is due to Wilson [1]. It has been widely studied but has the disadvantage of breaking explicitly chiral symmetry. Recent theoretical developments made it possible to have chiral fermions on the lattice. There are two equivalent formulations known as domain wall fermions [4, 5] and overlap fermions [6, 7]. They both require larger computer resources than Wilson fermions.

The vacuum expectation value of any gauge invariant operator \hat{O} can be computed by evaluating the path integral

$$\langle \Omega | \hat{O} | \Omega \rangle = \frac{\int d[U] d[\bar{\psi}] d[\psi] O[U, \bar{\psi}, \psi] e^{-S_g[U] - S_F[U, \bar{\psi}, \psi]}}{\int d[U] d[\bar{\psi}] d[\psi] e^{-S_g[U] - S_F[U, \bar{\psi}, \psi]}} \quad (1)$$

Integrating over the fermionic degrees of freedom we obtain

$$\langle \Omega | \hat{O} | \Omega \rangle = \frac{\int d[U] \det(D[U]) O[U, D^{-1}[U]] e^{-S_g[U]}}{Z} \quad Z \equiv \int d[U] \det(D[U]) e^{-S_g[U]} \quad , \quad (2)$$

where a factor $D_{jn}^{-1}[U]$ substitutes each appearance of $-\bar{\psi}_n \psi_j$ in O . One can now perform the path integrals numerically by stochastically generating a representative ensemble of gauge fields U according to the probability $\exp\{-S_g[U] + \ln(\det(D[U]))\} / Z$ and then compute

$$\langle \Omega | \hat{O} | \Omega \rangle = \lim_{N \rightarrow \infty} \frac{1}{N} \sum_{k=1}^N O[U^k, D^{-1}[U^k]] \quad , \quad (3)$$

which involves the evaluation of the inverse of the fermionic matrix. For a typical lattice of size $24^3 \times 48$ the dimension of the complex matrix D is 8 million by 8 million. Therefore the time consuming part of a lattice calculation is the generation of an ensemble of gauge configurations and the computation of the inverse of the fermionic matrix D which yields the quark propagator. In many applications only a column of D^{-1} is required.

The first lattice calculations were performed in the quenched approximation, which neglects pair creation by setting $\det(D) = 1$ in Eq. (2). This facilitates the generation of gauge links since one is left with the local action $S_g[U]$. In the quenched approximation the program outline above, i.e. taking the continuum and infinite volume limits and extrapolating to the physical quark masses, has been carried out for the spectrum of the low lying hadrons [8]. During the past five years theoretical progress in combination with terascale computers have made unquenched calculations with light pions and large enough volumes feasible [2, 9, 10, 11], using a number of different discretization schemes.

In order to study the role of the pion cloud, which is expected to provide an important ingredient in the description of the properties of the nucleon system, one must generate dynamical gauge configurations with light quarks using large volumes. In this work the light quark regime is studied in two ways:

1. We use configurations with the lightest available dynamical Wilson fermions. The unquenched configurations are simulated with two degenerate flavors of Wilson fermions [10, 11].
2. We use MILC configurations generated with two degenerate light and one strange staggered quarks using the Asqtad improved action [2]. For the valence quarks we use domain wall fermions that preserve chiral symmetry on the lattice. This is therefore a hybrid calculation that uses different fermions for the sea and valence quarks, i.e the matrix D appearing in the determinant in Eq. (2) is different from D^{-1} involved in the calculation of O in Eq. (3). Such hybrid calculations have been successful in recent evaluations of fundamental physical quantities such as g_A [12] and the pseudoscalar decay constants f_π and f_K [13].

Bearing in mind that both quenched and unquenched Wilson fermions have discretization errors of order a , and that both Asqtad and domain wall fermion actions have discretization errors of order a^2 and fermions preserving chirality,

in contrast to Wilson fermions, agreement between the results within these two different lattice fermion formulations provides a non-trivial check of consistency of the lattice results. The hybrid calculation is computationally the most demanding since it requires propagators on a five-dimensional lattice. The bare quark mass for the domain wall fermions, the size of the fifth dimension and the renormalization factors Z_V and Z_A for the four-dimensional vector and axial vector currents are taken from Ref. [12]. The parameters of our calculations are given in Table 1.

TABLE 1. We give the number of configurations, the hopping parameter, κ , which determines the bare quark mass via the relation $2am_q = (1/\kappa - 1/\kappa_c)$ for the case of Wilson fermions or the mass of the u and d quarks, m_l , for the case of staggered quarks, the pion, nucleon and Δ mass in lattice units with their statistical errors determined from a jackknife analysis. For Wilson fermions a is set using the nucleon mass at the chiral limit whereas for staggered fermions we take the value extracted from the static $q\bar{q}$ force as determined in Ref. [14].

no. of configurations	κ (Wilson) or am_l (staggered)	am_π	aM_N	aM_Δ
Quenched $32^3 \times 64$ $a^{-1} = 2.14(6)$ GeV				
200	0.1554	0.263(2)	0.592(5)	0.687(7)
200	0.1558	0.229(2)	0.556(6)	0.666(8)
200	0.1562	0.192(2)	0.518(6)	0.646(9)
	$\kappa_c = 0.1571$	0.	0.439(4)	0.598(6)
Unquenched Wilson $24^3 \times 40$ $a^{-1} = 2.56(10)$ GeV				
185	0.1575	0.270(3)	0.580(7)	0.645(5)
157	0.1580	0.199(3)	0.500(10)	0.581(14)
Unquenched Wilson $24^3 \times 32$ $a^{-1} = 2.56(10)$ GeV				
200	0.15825	0.150(3)	0.423(7)	0.533(8)
	$\kappa_c = 0.1585$	0.	0.366(13)	0.486(14)
MILC $20^3 \times 64$ $a^{-1} = 1.58$ GeV				
150	0.03	0.373(3)	0.886(7)	1.057(14)
150	0.02	0.306(3)	0.800(10)	0.992(16)
MILC $28^3 \times 64$ $a^{-1} = 1.58$ GeV				
118	0.01	0.230(3)	0.751(7)	0.988(26)

The main goal of this program is to calculate within lattice QCD the fundamental physical quantities of the nucleon- Δ system. Providing the complete set of form factors and coupling constants constitutes a very important input for model builders and for fixing the parameters of chiral effective theories. In this presentation we discuss our results for the nucleon elastic form factors and the electromagnetic and axial N to Δ transition form factors as well as show first results on their wave functions. Other recent lattice studies on nucleon properties can be found in Ref. [15].

II. LATTICE TECHNIQUES

The vacuum expectation value of gauge invariant operators is computed by numerical evaluation of appropriately defined path integrals. Let us first consider the evaluation of hadron masses. The vacuum expectation value of the time ordered product $G^h(t, \mathbf{q}) = \langle \Omega | \sum_{\mathbf{x}} \exp(i\mathbf{q} \cdot \mathbf{x}) \hat{T} \hat{J}_h(\mathbf{x}, t) \hat{J}_h^\dagger(0) | \Omega \rangle$ can be evaluated using Eqs. (2) and (3) which require inverting D for each non-degenerate quark flavor once per gauge configuration. The interpolating fields, $\hat{J}_h(x)$ are operators in the Heisenberg representation that create a trial state with the quantum numbers, h , of the hadron that we want to study. For example in the nucleon case an appropriate interpolating field is $\hat{J}_N(x) = \epsilon_{abc} [u_a^T(x) C \gamma_5 d_b(x)] u_c(x)$ where C is the charge conjugation operator and Latin indices denote color quantum numbers. The large time behavior of the correlator $G^h(t, \mathbf{0})$ yields the mass:

$$\begin{aligned}
G^h(t, \mathbf{q}) &= \sum_{n, \mathbf{p}} \sum_{\mathbf{x}} e^{-i\mathbf{q} \cdot \mathbf{x}} \langle \Omega | e^{\hat{H}t} e^{-i\hat{\mathbf{p}} \cdot \mathbf{x}} \hat{J}_h e^{-\hat{H}t} e^{i\hat{\mathbf{p}} \cdot \mathbf{x}} | n, \mathbf{p} \rangle \langle n, \mathbf{p} | \hat{J}_h^\dagger | \Omega \rangle = \sum_n | \langle \Omega | \hat{J}_h | n, \mathbf{q} \rangle |^2 e^{-E_n(\mathbf{q})t} \\
G^h(t, \mathbf{0}) &\stackrel{t(m_{h_1} - m_{h_0}) \gg 1}{\implies} | \langle \Omega | \hat{J}_h | h_0, \mathbf{0} \rangle |^2 e^{-m_{h_0}t}
\end{aligned} \tag{4}$$

where $E_n(\mathbf{q}) = \sqrt{m_n^2 + \mathbf{q}^2}$, $|h_0\rangle$ is the lowest eigenstate of QCD with quantum numbers h with mass m_{h_0} and we have taken $\mathbf{q} = \mathbf{0}$. For large time separation t between the source and the sink the unknown overlap factor $| \langle \Omega | \hat{J}_h | h_0, \mathbf{0} \rangle |^2$

and exponential dependence cancel in the ratio $m_{\text{eff}}(t) = -\log [G^h(t)/G^h(t-1)]$, which therefore becomes time independent and can be fitted to a constant to extract the mass, m_{h_0} , of the lowest state.

Three-point functions of the form $G^{hA\tilde{h}}(t, t_1; \mathbf{q}) = \langle \Omega | \sum_{\mathbf{x}, \mathbf{y}} e^{i\mathbf{q}\cdot\mathbf{x}} \hat{J}_h(\mathbf{y}, t) \hat{A}(\mathbf{x}, t_1) \hat{J}_h^\dagger(0) | \Omega \rangle$ are required for the evaluation of form factors. Inserting a complete set of hadronic states between operators in $G^{hA\tilde{h}}(t, t_1; \mathbf{q})$ as we did above for the extraction of hadron masses from two-point functions, we obtain

$$G^{hA\tilde{h}}(t, t_1; \mathbf{q}) = \sum_{k, n, \mathbf{p}', \mathbf{p}} \sum_{\mathbf{x}, \mathbf{y}} e^{i\mathbf{q}\cdot\mathbf{x}} \langle \Omega | \hat{J}_h | n, \mathbf{p}' \rangle e^{-E_n(\mathbf{p}')t} e^{i\mathbf{p}'\cdot\mathbf{y}} e^{E_n(\mathbf{p}')t_1} e^{-i\mathbf{p}'\cdot\mathbf{x}} \langle n, \mathbf{p}' | \hat{A} | k, \mathbf{p} \rangle e^{-E_n(\mathbf{p})t_1} e^{i\mathbf{p}\cdot\mathbf{x}} \langle k, \mathbf{p} | \hat{J}_h^\dagger | \Omega \rangle$$

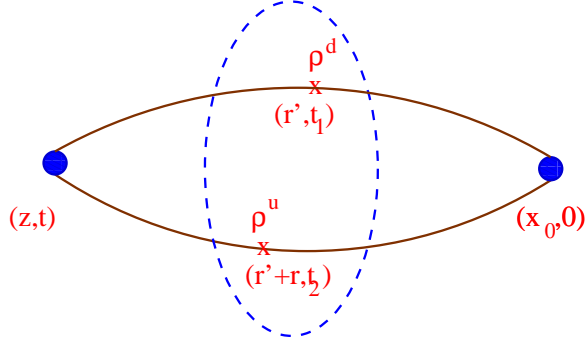
$$\stackrel{\Delta E(t-t_1) \gg 1, \Delta \tilde{E} t_1 \gg 1}{\implies} \langle \Omega | \hat{J}_h | h_0, \mathbf{0} \rangle \langle \tilde{h}_0, \mathbf{p} | \hat{J}_h^\dagger | \Omega \rangle \langle h_0, \mathbf{0} | \hat{A} | \tilde{h}_0, \mathbf{p} \rangle e^{-m_{h_0}(t-t_1)} e^{-E_{\tilde{h}_0}(\mathbf{p})t_1} \quad (5)$$

where ΔE and $\Delta \tilde{E}$ are the energy differences between the two lowest hadronic states with quantum numbers h and \tilde{h} and $\mathbf{p} = -\mathbf{q}$. The exponential time dependence and unknown overlaps can be canceled by dividing with appropriate combinations of two-point functions $G^h(t, \mathbf{q})$. For example in the ratio $R = G^{hA\tilde{h}}(t, t_1; \mathbf{q}) / \sqrt{G^h(2t - 2t_1, \mathbf{0}) G^{\tilde{h}}(2t_1, \mathbf{q})}$ the overlap factors and exponentials cancel in the large time limit when the ground states h_0 and \tilde{h}_0 dominate, yielding the matrix element $\langle h_0, \mathbf{0} | \hat{A} | \tilde{h}_0, \mathbf{p} \rangle$. Since both two- and three- point functions decay exponentially it is crucial in constructing the ratio to choose combinations of two-point functions that involve the shortest possible time separations and to use techniques that isolate the lowest hadronic states $|h_0\rangle$ and $|\tilde{h}_0\rangle$ at short time intervals. The former can be done by choosing better but more complicated ratios than the one given here, to be discussed in Sections IV and V [16, 17], whereas the latter by constructing better interpolating fields. Smearing techniques are routinely used for achieving ground state dominance before the signal from the time correlators is lost in the noisy large time limit. We use gauge invariant Wuppertal smearing to replace local by smeared quark operators at the source and the sink [18] and, when needed, we apply hypercubic averaging [19] of the gauge links that enter the construction of the Wuppertal smearing function. As can be seen from Eq. (5), to compute three-point functions two sums over the spatial volume are needed. Performing the Wick contractions on the quark level for the three-point function one finds expressions that involve the full inverse of the fermionic matrix D (all-to-all propagator). This is to be contrasted with two-point functions for which only one spatial sum enters and therefore only one column of D is needed. The technique to automatically do one of the spatial sums by using an appropriately defined input vector that uses one column of the inverse of D when inverting, is known as sequential inversion. One can choose which of the two sums to do first. In this work we do the sum over the sink \mathbf{y} . This requires that the quantum numbers of the sink are fixed but allows any operator \hat{A} with any momentum \mathbf{q} to be inserted. This means that with one sequential inversion one can extract the matrix element $\langle h_0, \mathbf{0} | \hat{A} | \tilde{h}_0, \mathbf{p} \rangle$ for given hadronic states but different operators and momentum \mathbf{q} . We therefore measure the matrix element for all lattice momentum vectors that result in a given momentum transfer squared q^2 , thereby obtaining many statistically independent evaluations of the same form factors reducing statistical noise.

III. PROBING HADRON WAVE FUNCTIONS

Our main motivation for studying density-density correlators is that they reduce, in the non-relativistic limit, to the wave function squared yielding detailed, gauge-invariant information on the internal structure of hadrons [20, 21]. The shape of hadrons, which is the topic of this workshop, is one such important quantity that can be directly studied. There are indications from experimental measurements of the quadrupole strength in the $\gamma^* N \rightarrow \Delta$ transition [22] that the nucleon and/or the Δ are deformed. Density-density correlators, shown schematically in Fig. 1, are four-point functions since they involve the insertion of two density operators. Four-point functions are technically harder to compute than three-point functions discussed in the previous Section. In particular, they require computation of all the spatial columns of the inverse of the fermionic matrix requiring L^3 inversions. A straight forward computation of such an inverse is therefore prohibitively expensive. In our first study [23], which we consider as a feasibility study, the density-density correlators were evaluated without explicit projection to zero momentum hadronic states. This means that higher momentum states are suppressed only by the Euclidean time evolution.

We have analyzed 220 quenched configurations at $\beta = 6.0$ for a lattice of size $16^3 \times 32$ obtained from the NERSC archive, using the Wilson Dirac operator with hopping parameter $\kappa = 0.15, 0.153, 0.154$ and 0.155 . Using the relation $2am_q = (1/\kappa - 1/\kappa_c)$, with the critical value $\kappa_c = 0.1571$, one can obtain the naive quark mass m_q . A physical dimensionless quantity that is sensitive to the value of the bare quark mass is the ratio of the pion mass to the rho mass, which at these values of κ , is 0.88, 0.84, 0.78 and 0.70 respectively. We fix the source and the sink for maximum time



$$D(\mathbf{r}, t_1, t_2) = \int d^3 r' \langle h | \rho^u(\mathbf{r}' + \mathbf{r}, t_2) \rho^d(\mathbf{r}', t_1) | h \rangle$$

$$\rho^f(\mathbf{r}, t) = : \bar{f}(\mathbf{r}, t) \gamma_0 f(\mathbf{r}, t) : \quad (6)$$

where for the density operator we use the normal order product so that disconnected graphs are excluded.

FIGURE 1. The density-density correlator, $D(\mathbf{r}, t_1, t_2)$, for a meson. The time separations t_1 , t_2 , $t - t_1$ and $t - t_2$ are taken large enough to isolate the mesonic ground state.

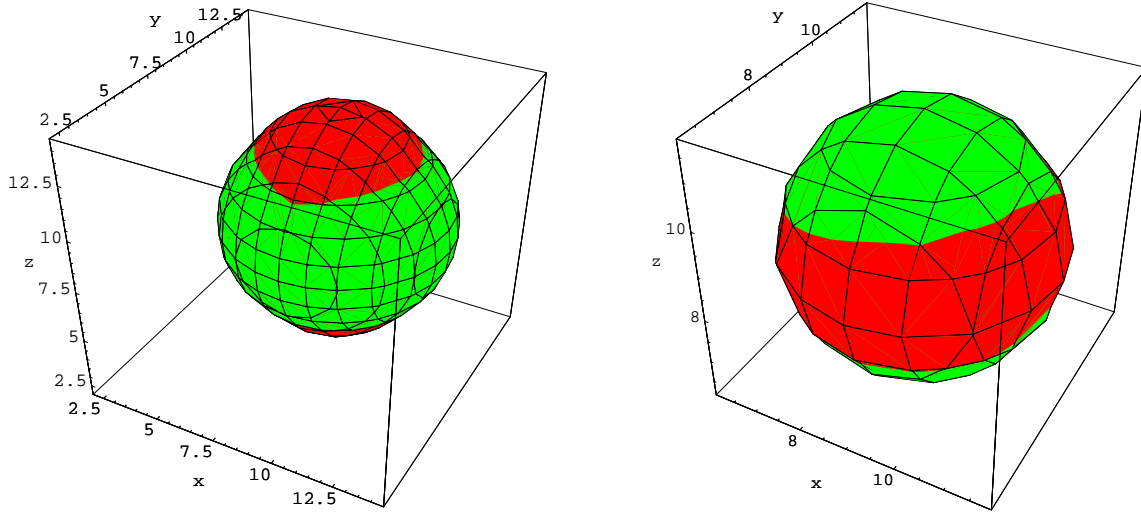


FIGURE 2. A three-dimensional contour plot of the correlator is shown in red. Left: for the rho state with 0 spin projection (cigar shape); Right: for the Δ^+ state with +3/2 (slightly oblate) spin projection for two dynamical quarks at $\kappa = 0.156$. Values of the correlator (0.5 for the rho, 0.8 for the Δ^+) were chosen to show large distances but avoid finite-size effects. We have included for comparison the contour of a sphere (green).

separation, which for this lattice is $t/a = 16$ given the antiperiodic boundary conditions in the time direction. Both density insertions are taken at the same time slice at the middle of the time interval. To investigate the importance of dynamical quarks, we use SESAM configurations [24] generated with two dynamical degenerate quark species at $\beta = 5.6$ on a lattice of size $16^3 \times 32$ at $\kappa = 0.156$ and 0.157 . The ratio of the pion mass to rho mass is 0.83 at $\kappa = 0.156$ and 0.76 at $\kappa = 0.157$. These values are close to the quenched mass ratios measured at $\kappa = 0.153$ and $\kappa = 0.154$ respectively, allowing us to make pairwise quenched-unquenched comparisons. The general conclusion of this comparison is that, at these heavy quark masses, unquenching effects are small. We show in Fig. 2 contour plots of the density-density correlator for the rho and the Δ for the case of dynamical Wilson fermions at the heavy quark mass. The elongation in the rho is clearly visible whereas the Δ^+ appears to be squeezed.

We have recently developed techniques for the evaluation of density-density correlators with explicit projection to zero momentum hadronic states [25] and we are in the process of analyzing unquenched SESAM configurations at lighter quark masses as listed in Table 1.

IV. NUCLEON FORM FACTORS

Recent results from polarization experiments [26, 27], have shown a qualitative different behavior than the traditional Rosenbluth separation for the ratio of the proton electric to magnetic form factor, $\mu_p G_E^p/G_M^p$. An accurate determination of these form factors in lattice QCD can provide an important theoretical input for understanding the q^2 -dependence of this ratio. We present here results obtained using Wilson fermions on the quenched and unquenched lattices given in Table 1. The smallest q^2 -values are accessible on the quenched lattice, which has the largest spatial extent, since the smallest available non-zero momentum on a finite lattice is $2\pi/L$ giving $-q^2 \sim 0.17 \text{ GeV}^2$. Although large momentum transfers are in principle available on typical lattices, the Fourier transform of two- and three-point functions becomes noise-dominated for momentum transfers beyond about 2 GeV^2 , limiting the range of high q^2 values that can be extracted accurately.

The standard decomposition of the nucleon electromagnetic matrix element for real or virtual photons is given by

$$\langle N(p', s') | j_\mu | N(p, s) \rangle = \left(\frac{M_N^2}{E_N(\mathbf{p}') E_N(\mathbf{p})} \right)^{1/2} \bar{u}(p', s') \left[\gamma_\mu F_1(q^2) + \frac{i\sigma_{\mu\nu} q^\nu}{2M_N} F_2(q^2) \right] u(p, s), \quad (7)$$

where $p(s)$ and $p'(s')$ denote initial and final momenta (spins), M_N is the nucleon mass, $F_1(0) = 1$ for the proton since we have a conserved current and $F_2(0)$ measures the anomalous magnetic moment. They are connected to the electric, G_E , and magnetic, G_M , Sachs form factors by the relations

$$G_E(q^2) = F_1(q^2) + \frac{q^2}{(2M_N)^2} F_2(q^2) \quad G_M(q^2) = F_1(q^2) + F_2(q^2) \quad . \quad (8)$$

The electromagnetic matrix element is extracted from the three-point function $G^{Nj_\mu N}$ following the procedure outline in the Section II. We use the lattice conserved electromagnetic current,

$$j^\mu(x) = \sum_{f=u,d} q_f \left[\bar{\psi}^f(x + \hat{\mu})(1 + \gamma_\mu) U_\mu^\dagger(x) \psi^f(x) - \bar{\psi}^f(x)(1 - \gamma_\mu) U_\mu(x) \psi^f(x + \mu) \right] \quad (9)$$

symmetrized on site x by taking $j^\mu(x) \rightarrow [j^\mu(x) + j^\mu(x - \hat{\mu})]/2$. We look for a plateau in the large Euclidean time behavior of the improved ratio

$$R(t, t_1; \mathbf{q}; \Gamma; \mu) = \frac{\langle G^{Nj_\mu N}(t, t_1; \mathbf{q}; \Gamma) \rangle}{\langle G^N(t, \mathbf{0}; \Gamma_4) \rangle} \left[\frac{\langle G^N(t_2 - t_1, \mathbf{p}; \Gamma_4) \rangle \langle G^N(t_1, \mathbf{0}; \Gamma_4) \rangle \langle G^N(t, \mathbf{0}; \Gamma_4) \rangle}{\langle G^N(t_2 - t_1, \mathbf{0}; \Gamma_4) \rangle \langle G^N(t_1, \mathbf{p}; \Gamma_4) \rangle \langle G^N(t, \mathbf{p}; \Gamma_4) \rangle} \right]^{1/2} \stackrel{\Delta E(t-t_1) \gg 1, \Delta E t_1 \gg 1}{\Rightarrow} \Pi(\mathbf{q}; \Gamma; \mu) \quad . \quad (10)$$

where we show explicitly the dependence on the projection matrices $\Gamma_j = \frac{1}{2} \begin{pmatrix} \sigma_j & 0 \\ 0 & 0 \end{pmatrix}$, $j = 1, 2, 3$ and $\Gamma_4 = \frac{1}{2} \begin{pmatrix} I & 0 \\ 0 & 0 \end{pmatrix}$ for the Dirac indices. ΔE is the energy difference between the nucleon and its excited P_{11} -state and $\mathbf{q} = -\mathbf{p}$ for a nucleon at rest in the final state. Since we want to study the q^2 -dependence of the form factors we evaluate the three point function with sequential inversion through the sink. We fix the source-sink time separation $t/a = 11(12)$ for the quenched (unquenched) Wilson lattices and search for a plateau of $R(t, t_1; \mathbf{q}; \Gamma; \mu)$ as a function of the time slice, t_1 , at which j_μ couples to a quark. $Q^2 = -q^2$ denotes the Euclidean momentum transfer squared.

The two Sachs form factors are extracted from the ratio defined in Eq. (10) by choosing appropriate combinations of the direction μ of the electromagnetic current and projection matrices Γ . Provided the Euclidean time separations t_1 and $t - t_1$ are large enough to filter the nucleon ground state, the ratio $R(t, t_1; \mathbf{q}; \Gamma; \mu)$ becomes time independent and the two form factors can be extracted from the Euclidean space expressions,

$$\sum_{k=1}^3 \Pi(\mathbf{q}; \Gamma_k; \mu = i) = \frac{K}{2M_N} \left\{ (p_2 - p_3) \delta_{1,i} + (p_3 - p_1) \delta_{2,i} + (p_1 - p_2) \delta_{3,i} \right\} G_M(Q^2) \quad (11)$$

$$\Pi(\mathbf{q}; \Gamma_4; \mu = i) = K \frac{q_i}{2M_N} G_E(Q^2) \quad , \quad \Pi(\mathbf{q}; \Gamma_4; \mu = 4) = K \frac{E_N + M_N}{2M_N} G_E(Q^2) \quad (12)$$

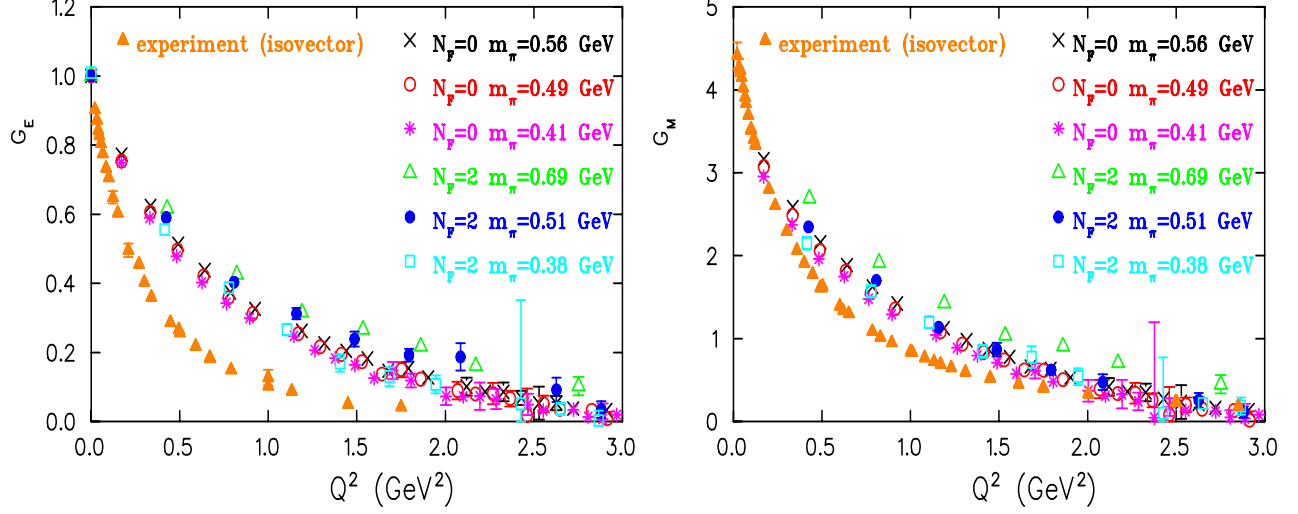


FIGURE 3. The isovector form factors, G_E , (right) and G_M , (left) as a function of Q^2 . By $N_F = 0$ we denote quenched lattice results at $\kappa = 0.1554$ (crosses), at $\kappa = 0.1558$ (open circles) and at $\kappa = 0.1562$ (asterisks). Results using two degenerate flavors of dynamical Wilson fermions are denoted by $N_F = 2$ at $\kappa = 0.1575$ (open triangles), $\kappa = 0.1580$ (filled circles) and at $\kappa = 0.15825$ (open squares). The filled triangles show experimental results for the isovector form factors extracted by interpolating the experimental data for the proton and neutron form factors (the details of the interpolations are given in Ref. [17]).

where $K = \sqrt{\frac{2M_N^2}{E_N(E_N+M_N)}}$ is a factor due to the normalization of the lattice states. We note that the expression for G_M is obtained by using an optimal linear combination for the nucleon sink that provides the maximal set of lattice measurements from which G_M can be extracted requiring only one sequential inversion. Eqs. (12) yield G_E with an additional sequential inversion.

The $\gamma^*N \rightarrow N$ transition, in addition to an isovector part, contains isoscalar photon contributions. This means that disconnected loop diagrams also contribute. These are generally difficult to evaluate accurately since the all-to-all quark propagator is required. In order to avoid disconnected diagrams, we calculate the isovector form factors. Assuming $SU(2)$ isospin symmetry, it follows that

$$\langle p | (\frac{2}{3}\bar{u}\gamma^\mu u - \frac{1}{3}\bar{d}\gamma^\mu d) | p \rangle - \langle n | (\frac{2}{3}\bar{u}\gamma^\mu u - \frac{1}{3}\bar{d}\gamma^\mu d) | n \rangle = \langle p | (\bar{u}\gamma^\mu u - \bar{d}\gamma^\mu d) | p \rangle. \quad (13)$$

One can therefore calculate directly the three-point functions related to the right hand side of the above relation, from which the *isovector* nucleon form factors

$$G_E(q^2) = G_E^p(q^2) - G_E^n(q^2), \quad G_M(q^2) = G_M^p(q^2) - G_M^n(q^2) \quad , \quad (14)$$

can be extracted using Eqs. (11) and (12) by only evaluating connected diagrams.

Besides using an optimal nucleon source, the other important ingredient in the extraction of the form factors, is to take into account simultaneously in our analysis all the lattice momentum vectors that contribute to a given Q^2 . This is done by solving the overcomplete set of equations $P(\mathbf{q}; \mu) = A(\mathbf{q}; \mu) \cdot F(Q^2)$ where $P(\mathbf{q}; \mu)$ are the lattice measurements of the ratio given in Eq. (10) having statistical errors w_k and using the different sink types, $F = \begin{pmatrix} G_E \\ G_M \end{pmatrix}$ and A is an $M \times 2$ matrix which depends on kinematical factors with M being the number of current directions and momentum vectors contributing to a given Q^2 . We extract the form factors by minimizing

$$\chi^2 = \sum_{k=1}^N \left(\frac{\sum_{j=1}^2 A_{kj} F_j - P_k}{w_k} \right)^2 \quad (15)$$

using the singular value decomposition of the matrix A . Given the fact that one can have a few hundred lattice momentum vectors contributing for a given Q^2 , the statistical precision is highly improved. There is an additional

advantage arising from including momentum vectors \mathbf{q} as well as $-\mathbf{q}$ in our analysis: The lattice conserved current given in Eq. (9) differs from the local electromagnetic current $\bar{\psi}(x)\gamma_\mu\psi(x)$ by terms of order a . However when we average over \mathbf{q} and $-\mathbf{q}$ these order a terms vanish.

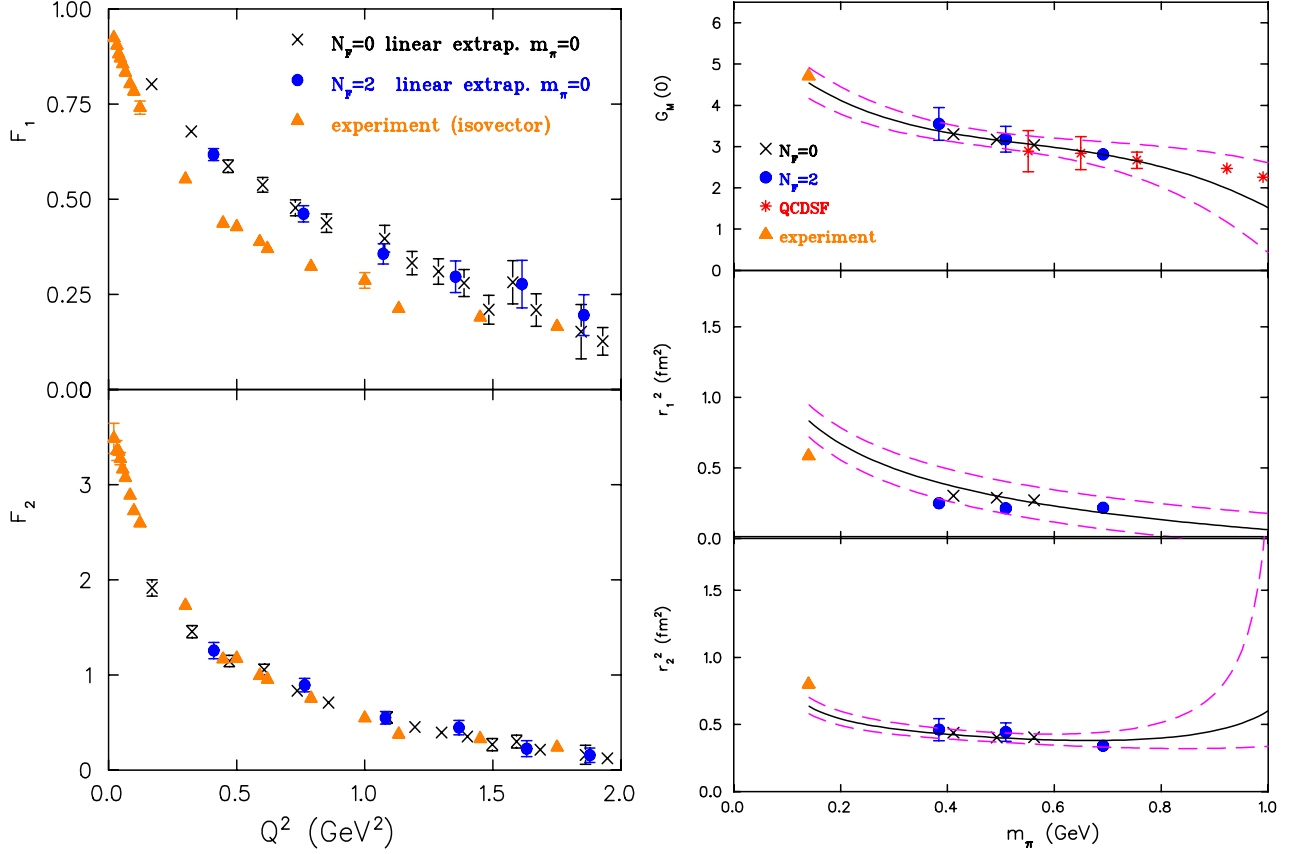


FIGURE 4. Left: The form factors F_1 (upper) and F_2 (lower) as a function of Q^2 at the chiral limit. The results extracted from experiment are shown by the filled triangles. Right: Chiral extrapolation of the magnetic moment (upper) and the r.m.s radii r_1 (middle) and r_2 (lower). The solid line is the best fit to the effective chiral theory results. The dashed lines show the maximal allowed error band using the errors on the fitted parameters. In all graphs quenched results are shown by the crosses and unquenched results by the filled circles. Quenched results from Ref. [28] are shown by the asterisks.

In Fig. 3 we show quenched and unquenched results for the isovector electric and magnetic form factors using Wilson fermions at the three values of the quark mass given in Table 1. Both quenched and unquenched results decrease with the quark mass yielding a larger slope at small Q^2 , which is the expected behavior. However both quenched and unquenched results for G_E deviate more from experiment than G_M for the same quark mass. The two main uncertainties regarding lattice results are finite a -effects and the fact that the u- and d- quark masses are larger than physical. In the quenched theory one can envisage repeating the calculation using a finer lattice in order to check whether finite a -effects can explain this behavior. Evaluation of these form factors closer to the chiral limit with Wilson fermions is problematic and one will have to use other types of discretization for the fermions to study the dependence on lighter quark masses. To be able to directly compare with experiment, using the results of this work, we need to extrapolate G_E and G_M to the chiral limit. The quark masses employed in this work correspond to pion masses in the range 560 to 410 MeV in the quenched theory and 690 to 380 MeV in the unquenched theory. Pion cloud effects are expected to be small in this range of pion masses and therefore we expect a linear dependence of the results on m_π^2 . Our lattice data at these quark masses confirm this expectation and therefore, to obtain results in the chiral limit, we extrapolate the form factors linearly in m_π^2 . We show the linearly extrapolated lattice results for F_1 and F_2 in Fig. 4. We observe agreement between quenched and unquenched results at the chiral limit. In addition, there is good agreement between lattice results for F_2 and experiment, with perhaps small deviations at small Q^2 . This is not the case for F_1 where the experimentally determined isovector F_1 decays faster as compared to the lattice results. In a recent calculation, the quark mass dependence of the isovector magnetic moment and radii was determined. This was done

within a chiral effective theory with explicit nucleon and Δ degrees of freedom [28, 29]. Therefore we can extract the relevant low energy constants and counterterms that enter in the expressions of these quantities in the effective chiral theory from fits to our form factors and obtain results at the physical pion mass. Fitting to our lattice data we obtain the curve shown by the solid line in Fig. 4. The details regarding the fits are given in Ref. [17]. The dashed lines give the maximal error band determined by varying the values of the fitted parameters by their errorbars. The extrapolated value of the magnetic moment at the physical pion mass is in agreement with experiment. The resulting fits for the radii are also shown in Fig. 4. The pion mass dependence of the Dirac radius is not well reproduced. Since this is related to the slope of F_1 this is not surprising given that the lattice results have a different slope from the experimental results and hardly show any quark mass dependence.

V. N TO Δ TRANSITION FORM FACTORS

The evaluation of the N- Δ matrix element, within the fixed sink approach, requires a new set of sequential propagators since in the final state, instead of the nucleon, we have the Δ . However, once we produce the sequential propagators needed for the evaluation of the electromagnetic N- Δ matrix element, the axial one can be obtained with almost no additional computational cost using the same sequential propagators. The N to Δ transition involves no disconnected diagrams and therefore lattice results can be directly compared to experiment.

V.1. Electromagnetic transition form factors

To address the question of possible deformation in the nucleon system the experiment of choice is electroproduction of the Δ that measures the nucleon- Δ transition amplitudes. Non-zero quadrupole amplitudes are thought to be connected with a non-spherical nucleon or/and Δ [22]. We can establish direct contact with experiment by calculating the N to Δ transition form factors in lattice QCD. To obtain accurate results that can provide a meaningful comparison to experiment two novel aspects are implemented: 1) An optimal combination of three-point functions, which allows momentum transfers in a spatially symmetric manner obtained by an appropriate choice of the interpolating field for the Δ . This is similar to the construction of the optimal nucleon source for the calculation of the nucleon magnetic form factor, G_M , discussed in the previous Section but more involved [16]. 2) An overconstrained analysis using all lattice momentum vectors contributing to a given q^2 value in the extraction of the three transition form factors analogous to what was done for the elastic nucleon form factors.

The matrix element for the $\gamma^* N \rightarrow \Delta$ transition with on-shell nucleon and Δ states and real or virtual photons has the form [30]

$$\langle \Delta(p', s') | j^\mu | N(p, s) \rangle = i \sqrt{\frac{2}{3}} \left(\frac{m_\Delta m_N}{E_\Delta(\mathbf{p}') E_N(\mathbf{p})} \right)^{1/2} \bar{u}_\sigma(p', s') \mathcal{O}^{\sigma\mu} u(p, s) \quad (16)$$

where $u_\sigma(p', s')$ is a spin-vector in the Rarita-Schwinger formalism. $\mathcal{O}^{\sigma\mu}$ can be decomposed in terms of the Sachs form factors as

$$\mathcal{O}^{\sigma\mu} = \mathcal{G}_{M1}(q^2) K_{M1}^{\sigma\mu} + \mathcal{G}_{E2}(q^2) K_{E2}^{\sigma\mu} + \mathcal{G}_{C2}(q^2) K_{C2}^{\sigma\mu}, \quad (17)$$

where the magnetic dipole, \mathcal{G}_{M1} , the electric quadrupole, \mathcal{G}_{E2} , and the Coulomb quadrupole, \mathcal{G}_{C2} , form factors depend on the momentum transfer $q^2 = (p' - p)^2$. The kinematical functions $K^{\sigma\mu}$ in Euclidean space are given in ref. [31]. The ratios R_{EM} or EMR and R_{SM} or CMR in the rest frame of the Δ are obtained from the Sachs form factors via

$$R_{EM} = -\frac{\mathcal{G}_{E2}(q^2)}{\mathcal{G}_{M1}(q^2)}, \quad R_{SM} = -\frac{|\mathbf{q}|}{2m_\Delta} \frac{\mathcal{G}_{C2}(q^2)}{\mathcal{G}_{M1}(q^2)}. \quad (18)$$

We look for a plateau in the large Euclidean time behavior of the optimized ratio

$$R_\sigma(t_2, t_1; \mathbf{q}; \Gamma; \mu) = \frac{\langle G_\sigma^{\Delta j^\mu N}(t_2, t_1; \mathbf{q}; \Gamma) \rangle}{\langle G_{ii}^\Delta(t_2, \mathbf{0}; \Gamma_4) \rangle} \left[\frac{\langle G^N(t_2 - t_1, \mathbf{p}; \Gamma_4) \rangle \langle G_{ii}^\Delta(t_1, \mathbf{0}; \Gamma_4) \rangle \langle G_{ii}^\Delta(t_2, \mathbf{0}; \Gamma_4) \rangle}{\langle G_{ii}^\Delta(t_2 - t_1, \mathbf{0}; \Gamma_4) \rangle \langle G^N(t_1, \mathbf{p}; \Gamma_4) \rangle \langle G^N(t_2, \mathbf{p}; \Gamma_4) \rangle} \right]^{1/2}. \quad (19)$$

To extract \mathcal{G}_{M1} we take the symmetric combination,

$$S_1(\mathbf{q}; \mu) = \sum_{\sigma=1}^3 \Pi_\sigma(\mathbf{q}; \Gamma_4; \mu) = iA \sum_{\sigma=1}^3 \varepsilon^{\sigma 4 \mu j} p^j \mathcal{G}_{M1}(Q^2) \quad (20)$$

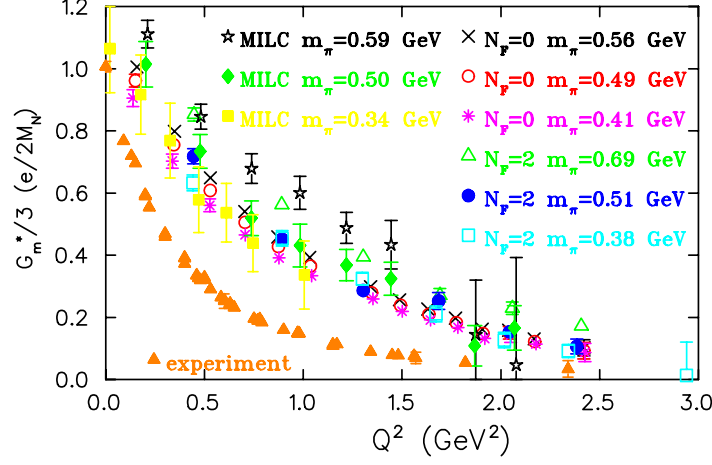


FIGURE 5. $G_m^*(Q^2) \equiv 1/\sqrt{1+Q^2/(m_N+m_\Delta)^2} \mathcal{G}_{M1}(Q^2)$ as function of Q^2 . The notation for Wilson fermions is the same as that in Fig. 3. Results within the hybrid scheme are shown with the stars for $m_l = 0.03$, with the filled rhombi for $m_l = 0.02$ and with the filled squares for $m_l = 0.01$. Experimental results from Ref. [32] are shown by the filled triangles.

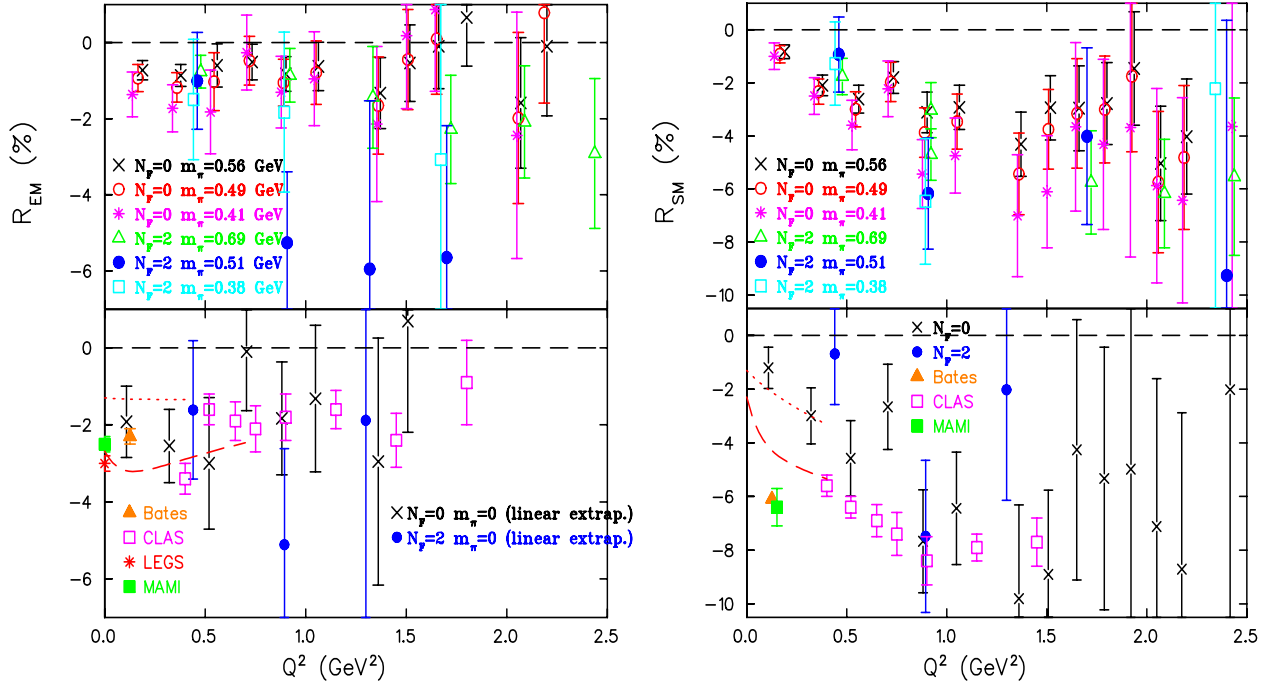


FIGURE 6. R_{EM} (left) and R_{SM} (right) as a function of Q^2 . Upper graphs show lattice results in the same notation as Fig. 3. The lower graphs show linear extrapolations to the chiral limit for quenched (crosses) and unquenched (filled circles) Wilson fermions. We include recent experimental results from Refs. [33] (filled triangle), [34] (open squares), [35] (asterisk), [36] (filled square). The dotted and dashed lines are the results from a dynamical model with bare and dressed vertices respectively [37].

computed for all spatial current directions so that lattice momentum vectors in all directions contribute. This combination, is built into the Δ interpolating field and requires only one inversion. Other combinations yield \mathcal{G}_{E2} and G_{C2} [16, 38, 39].

In Fig. 5 we show our results for the magnetic dipole form factor at similar pion masses for quenched and dynamical Wilson fermions and in the hybrid approach using MILC configurations and domain wall fermions. Comparing results for quenched and unquenched Wilson fermions we see that unquenching effects are small in this range of quark masses. We also observe agreement between the results obtained in the two dynamical calculations. As we have already pointed

out, agreement between the results using dynamical Wilson fermions and domain wall fermions is non-trivial since these discretization schemes have different lattice systematics. In all cases \mathcal{G}_{M1} decreases with the quark mass bringing lattice results closer to experiment. However, assuming a linear dependence in m_π^2 to extrapolate lattice data obtained using Wilson fermions where the statistical errors are the smallest, we find results at the chiral limit, which are higher than experiment. Module finite a -effects, the conclusion is that to reconcile lattice results with experiment a stronger dependence on m_π^2 for small quark masses seems necessary. In the hybrid approach the errors are larger and a reduction in the errors by at least a factor of two is required in order to draw any concrete conclusions regarding whether they show a better agreement with experiment.

Results for the EMR and CMR ratios are only shown for Wilson fermions in Fig. 6 since the errors on these ratios calculated in the hybrid scheme are too large prohibiting a meaningful comparison to the Wilson results. Although the results from dynamical Wilson fermions have larger errors than in the quenched case they tend to favor negative non-zero values for both ratios. However, given the size of the errors, an order of magnitude more configurations need to be analyzed in order to assess unquenching effects and draw a definite conclusion about the values of these ratios in the unquenched case. An analysis within a chiral effective theory leads to a non-trivial quark mass dependence for these ratios [40] that brings quenched lattice data in agreement with experiment at the lowest Q^2 -value.

V.2. Axial form factors

The N to Δ transition, besides being used to probe electromagnetic properties of the nucleon system, is also well suited for studying the weak structure functions. This is because the $\Delta(1232)$, as the dominant nucleon resonance, can be well identified and being a purely isovector spin-flip transition, provides selective information on hadron structure. A lattice calculation of the axial form factors is timely and important given that experiments at Jefferson Lab [41] are underway to measure these form factors. In this work we evaluate the dominant contribution to the parity violating asymmetry, which is determined by the ratio C_5^A/C_3^V and is to be measured at Jefferson Lab. This ratio is the off-diagonal analog of the g_A/g_V ratio extracted from neutron β -decay and therefore tests low-energy consequences of chiral symmetry, such as the off-diagonal Goldberger-Treiman relation. In addition the ratio of axial form factors C_6^A/C_5^A provides a measure for the conservation of the axial current [42].

The invariant N to Δ weak matrix element can be expressed in terms of four transition form factors as [43, 44]:

$$\begin{aligned} \langle \Delta(p', s') | A_\mu^3 | N(p, s) \rangle &= i\sqrt{\frac{2}{3}} \left(\frac{M_\Delta M_N}{E_\Delta(\mathbf{p}') E_N(\mathbf{p})} \right)^{1/2} \bar{u}^\lambda(p', s') \left[\left(\frac{C_3^A(q^2)}{M_N} \gamma^\nu + \frac{C_4^A(q^2)}{M_N^2} p^\nu \right) (g_{\lambda\mu} g_{\rho\nu} - g_{\lambda\rho} g_{\mu\nu}) q^\rho \right. \\ &\quad \left. + C_5^A(q^2) g_{\lambda\mu} + \frac{C_6^A(q^2)}{M_N^2} q_\lambda q_\mu \right] u(p, s) \end{aligned} \quad (21)$$

where $A_\mu^3(x) = \bar{\psi}(x) \gamma_\mu \gamma_5 \frac{\tau^3}{2} \psi(x)$ is the isovector part of the axial current (τ^3 being the third Pauli matrix). Having evaluated the electromagnetic N to Δ transition form factors on the lattice this matrix element can be evaluated without requiring any further inversions since the optimized Δ sources are the same as those used in our study of the electromagnetic N to Δ transition and only the operator that couples to a quark line differs. We consider the same ratio as that given in Eq. 19 but replace the three-point function $G_\sigma^{\Delta j\mu N}(t, t_1; \mathbf{q}; \Gamma)$ with $G_\sigma^{\Delta A_\mu^3 N}(t, t_1; \mathbf{q}; \Gamma)$. In the large Euclidean time limit this ratio yields the transition matrix element of Eq. (21). Using, for example, the Δ source, S_1 , for the evaluation of the three-point function we obtain for large time separations t_1 and $t - t_1$

$$S_1(\mathbf{q}, \mu = 4) = B \sum_{k=1}^3 p^k \left[C_3^A + \frac{M_\Delta}{M_N} C_4^A + \frac{E_N - M_\Delta}{M_N} C_6^A \right] \quad (22)$$

where the kinematical constants $B = B' / [3(m_\Delta + m_N)]$ and $B' = \sqrt{2/3} (M_\Delta/M_N + 1) \sqrt{(E_N(\mathbf{p}) + M_N)/E_N(\mathbf{p})}$ and with kinematics where the Δ is produced at rest. Using S_1 and the other sink types used in our study of the electromagnetic form factors [38, 42] the four axial form factors C_3^A , C_4^A , C_5^A and C_6^A can be determined by performing an overconstrained analysis as described in Section IV.

In Fig. 7 we show our lattice results for the four axial form factors for Wilson fermions and in the hybrid scheme. For the Wilson fermions we use $Z_A = 0.8$ [45, 46]. In all cases we observe that C_3^A is consistent with zero. Comparison

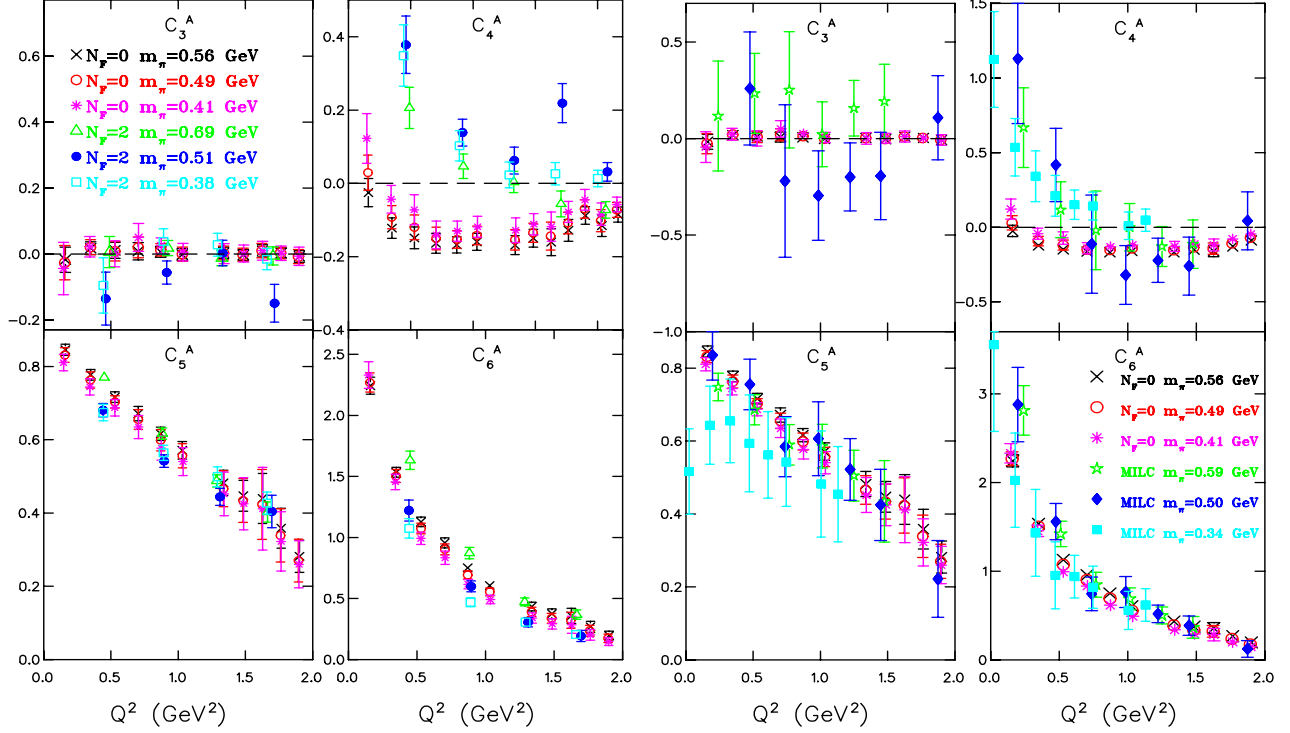


FIGURE 7. The axial form factors C_3^A , C_4^A , C_5^A and C_6^A as a function of Q^2 . The notation is the same as that in Fig. 5.

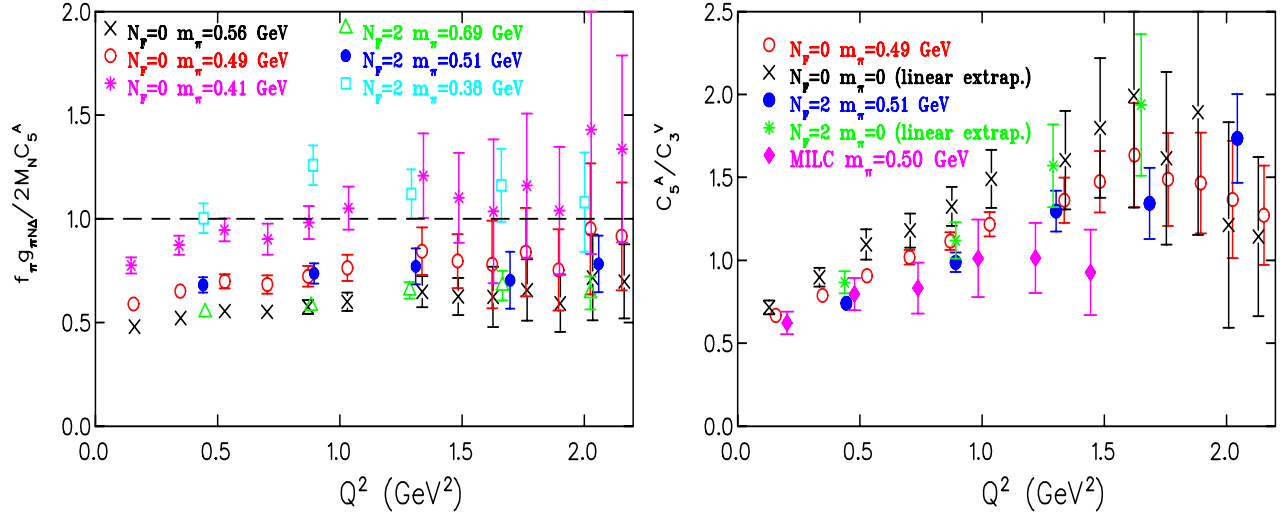


FIGURE 8. Left: The ratio $f_\pi g_{\pi N \Delta} / (2 M_N C_5^A)$ is shown versus Q^2 for Wilson fermions in the same notation as that of Fig. 3. Right: The ratio C_5^A / C_3^V is shown versus Q^2 at $\kappa = 0.1558$ (open circles) and at the chiral limit (crosses) for quenched QCD, at $\kappa = 0.1580$ (filled circles) and at the chiral limit (asterisks) for dynamical Wilson fermions and at $am_l = 0.02$ (filled rhombi) for domain wall fermions.

of quenched and unquenched results obtained with Wilson fermions shows that unquenching effects are small for the dominant form factors, C_5^A and C_6^A . The form factor C_4^A shows an interesting behavior: The unquenched results for both dynamical Wilson and domain wall fermions show an increase at low momentum transfers. Such large deviations between quenched and full QCD results for these relatively heavy quark masses are unusual making this an interesting quantity to study effects of unquenching.

For finite mass pions partial conservation of axial current ($\partial^\mu A_\mu^a(x) = f_\pi m_\pi^2 \pi^a(x)$) leads to the off-diagonal Goldberger-Treiman relation $C_5^A(Q^2) = f_\pi g_{\pi N\Delta}(Q^2)/2M_N$ where $g_{\pi N\Delta}(Q^2)$ is determined from the matrix element of the pseudoscalar density $\langle \Delta^+ | \bar{\psi}(x) \gamma_5 \frac{\tau_3}{2} \psi(x) | p \rangle$ and the pion decay constant f_π from the two-point function $\langle 0 | A_4(x) | \pi \rangle$. To relate the lattice pion matrix element to its physical value we need the pseudoscalar renormalization constant, Z_p . For quenched [45] and dynamical Wilson fermions [46] $Z_p(\mu^2 a^2 \sim 1) = 0.5$, which however may depend on the renormalization scale. At the chiral limit, at the lowest available momentum, we find $g_{\pi N\Delta}(Q^2 = 0.135 \text{ GeV}^2) = 18.0(1.9)$ and $g_{\pi N\Delta}(Q^2 = 0.443 \text{ GeV}^2) = 15.8(1.8)$ for quenched and dynamical Wilson fermions respectively where the quoted errors include a 10% uncertainty in Z_p . These values are to be compared with $g_{\pi N\Delta}(m_\pi^2) = 23.2 \pm 2.6$ obtained from an analysis of πN scattering [47]. We show in Fig. 8 the ratio $f_\pi g_{\pi N\Delta} / (2M_N C_5^A)$ for Wilson fermions. We observe that this ratio is almost independent of Q^2 and that, as the quark mass decreases, it becomes consistent with unity in agreement with the off-diagonal Goldberger-Treiman relation.

A prediction of lattice QCD is the ratio C_5^A/C_3^V . The form factor C_3^V can be obtained from the electromagnetic N to Δ transition. Using our lattice results for the dipole and electric quadrupole Sachs factors, \mathcal{G}_{M1} and \mathcal{G}_{E2} , we extract C_3^V using the relation

$$C_3^V = \frac{3}{2} \frac{M_\Delta(M_N + M_\Delta)}{(M_N + M_\Delta)^2 + Q^2} (\mathcal{G}_{M1} - \mathcal{G}_{E2}). \quad (23)$$

The ratio C_5^A/C_3^V , shown in Fig. 8 for $m_\pi \sim 500$ MeV, has values that fall within errorbars in the quenched theory and in full QCD. Given this agreement between quenched and unquenching results in this quark mass range, we opt to extrapolate the quenched results, which carry the smallest errors, to the chiral limit. As can be seen from Fig. 8 a linear extrapolation in m_π^2 leads to only a small increase in this ratio at the chiral limit. Without an analysis within a chiral effective theory for the quark mass dependence, this is the best that can be done to extract a reasonable estimate for the physical value of this ratio. Under certain assumptions, such as taking $C_3^A \sim 0$ and considering that C_4^A is suppressed as compared to C_5^A , both of which are justified by the lattice results, the parity violating asymmetry can be shown to be proportional to this ratio [48]. Our lattice results show that this ratio and, to a first approximation the parity violating asymmetry, is non-zero at $Q^2 = 0$ and increases by a factor of 2-3 when $Q^2 \sim 1.5 \text{ GeV}^2$.

VI. CONCLUSIONS

State-of-the-art lattice QCD calculations yield accurate results on a number of observables that are important for understanding the structure of the nucleon. We have presented the framework of such lattice computations for the nucleon and N to Δ transition form factors for quenched and dynamical Wilson fermions. The results are accurate enough to allow a meaningful comparison to experiment. We also evaluated the N to Δ transition form factors within a hybrid scheme, that combines the best simulation of the QCD vacuum that is available up to now using staggered fermions, with domain wall fermions that have good chiral properties. Within this hybrid scheme, we obtain results which are consistent with those obtained with dynamical Wilson fermions, albeit with larger statistical errors. Although chiral fermions are more expensive, smaller quark masses can be reached without any conceptual difficulties. Work is in progress to calculate the Δ form factors and coupling constants within the same framework. The aim of this program is to evaluate a complete set of observables for the nucleon- Δ system at small enough quark masses so that one can use only lattice input to fix the parameters of chiral effective theories. Extrapolation to the physical regime can then be carried out avoiding uncontrolled approximations. Dynamical Wilson and MILC configurations at pion masses of 250 MeV on large enough volumes are now becoming available and therefore, using the technology developed, we will be able to calculate these quantities closer to the chiral limit where we can reliably make contact with chiral perturbation expansions.

ACKNOWLEDGMENTS

I am indebted to my collaborators R. Edwards, Ph. de Forcrand, G. Koutsou, Th. Leontiou, Th. Lippert, H. Neff, J. W. Negele, K. Schilling, W. Schroers and A. Tsapalis for their valuable input to this work. I would like to thank C. N. Papanicolas for bringing to my attention the experimental efforts to understand hadron deformation and for providing the motivation and encouragement to undertake the lattice QCD studies. The computations were partly carried out on the IBM machines at NIC, Julich, Germany and at the National Energy Research Scientific Computing Center (NERSC), which is supported by the Office of Science of the U.S. Department of Energy under Contract No.

DE-AC03-76SF00098. This work is supported in part by the EU Integrated Infrastructure Initiative Hadron Physics (I3HP) under contract RII3-CT-2004-506078.

REFERENCES

1. K. Wilson, Phys. Rev. **D 10**, 245 (1974).
2. C. Bernard *et al.*, Phys. Rev. **D61**, 111502R (2000), K. Orginos, D. Tousaint and R. L. Sugar, Phys. Rev. **D 60**, 054503 (1999).
3. F. Farchioni *et al.*, hep-lat/0512017; R. Frezzotti and G. Rossi, JHEP 0408, 007 (2004); JHEP 0410, 070 (2004).
4. D. Kaplan, Phys. Lett. **B288**, 342 (1992).
5. Y. Shamir, Nucl. Phys. **B406**, 90 (1993).
6. P. Hasenfratz and F. Nidermayer, Nucl. Phys. **B414**, 785 (1994).
7. R. Narayanan and H. Neuberger, Phys. Lett. **B302**, 62 (1993); Phys. Rev. Lett. **71** 3251 (1993); Nucl. Phys. **B412**, 412 (1994); Nucl. Phys. **B443**, 305 (1995).
8. S. Aoki *et al.* (JLQCD Collaboration), Phys. Rev. **D 68**, 054502 (2003).
9. A. Shindler, PoS LAT2005, 014 (2006); S. Capitani *et al.*, Phys. Lett **B639**, 520 (2006).
10. B. Orth, Th. Lippert and K. Schilling, Phys. Rev. **D 72**, 014503 (2005).
11. C. Urbach *et al.*, Comput. Phys. Commun. **174**, 87 (2006).
12. R. G. Edwards *et al.* (LPH Collaboration), Phys. Rev. Lett. **96**, 052001 (2006).
13. S. R. Beane, P. F. Bedaque, K. Orginos and M. J. Savage, hep-lat/0606023.
14. C. Aubin *et al.*, Phys. Rev. **D 70**, 094505 (2004).
15. J. W. Negele, (LHP Collaboration), Int. J. Mod. Phys **A21**, 729 (2006); M. Göckeler, *et al.* (QCDSF Collaboration), Nucl Phys. Proc. Suppl. **153**, 146 (2006); Nucl. Phys. **A755**, 537 (2005); G. Schierholz, AIP Conf. Proc. **747**, 227 (2005); D. B. Leinweber, *et al.*, Phys. Rev. Lett. **97**, 022001 (2006); S. Boinepalli, *et al.*, hep-lat/0604022; F. Berruto, *et al.*, Phys. Rev. **D73**, 054509 (2006); K. Orginos, Th. Blum and Sh. Ohta, Phys. Rev. **73**, 094503 (2006).
16. C. Alexandrou *et al.* Phys. Rev. Lett. **94**, 021601 (2005).
17. C. Alexandrou, G. Koutsou, J.W. Negele and A. Tsapalis, Phys. Rev. **D 74**, 034508 (2006).
18. , C. Alexandrou, *et al.*, Nucl. Phys. **B414**, 815 (1994); S. Güsken, Nucl. Phys. Proc. Suppl. **17**, 361 (1990).
19. A. Hasenfratz and F. Knechtli, Phys. Rev. **D 64**, 034504 (2001) .
20. M. Burkardt, J. M. Grandy and J. W. Negele, Annals Phys. **238**, 441 (1995).
21. W. Wilcox, Phys. Lett. **B289**, 411 (1992).
22. C. N. Papanicolas, Eur. Phys. J. **A18**, 141 (2003).
23. C. Alexandrou, Ph. de Forcrand and A. Tsapalis, Phys. Rev. **D 66** , 094503 (2002).
24. N. Eicker *et al.* (SESAM Collaboration), Phys. Rev. **D 59**, 014509 (1999).
25. C. Alexandrou *et al.*, PoS Latt2005, 030 (2006).
26. M. Jones *et al.* Phys. Rev. Lett. **84**, 1398 (2000); O. Gayou *et al.*, Phys. Rev. **C 64**, 038202 (2001); O. Gayou *et al.*, Phys. Rev. Lett. **88**, 092301 (2002).
27. C. E. Hyde-Wright and K. de Jager, Ann. Rev. Nucl. Part. Sci. **54**, 217 (2004).
28. M. Gockeler *et al.*, Phys. Rev. **D 71**, 034508 (2005).
29. T. R. Hemmert and W. Weise, Eur. Phys. J. **A 15**, 487 (2002).
30. H. F. Jones and M.C. Scadron, Ann. Phys. (N.Y.) **81**, 1 (1973).
31. C. Alexandrou *et al.*, Phys. Rev. **D 69**, 114506 (2004).
32. W. W. Ash *et al.*, Phys. Lett. **B24**, 165 (1967); D. Arndt and B. C. Tiburzi, Phys. Rev. **D 69**, 014501 (2004); W. Bartel *et al.*, Phys. Lett. **B28**, 148 (1968); J.C. Alder *et al.*, Nucl. Phys. **B 46**, 573 (1972); K. Bätzner *et al.*, Phys. Lett. **B39**, 575 (1972); S. Stein *et al.*, Phys. Rev. **D 12**, 1884 (1975).
33. C. Mertz *et al.*, Phys. Rev. Lett. **86**, 2663 (2001).
34. K. Joo *et al.*, Phys. Rev. Lett. **88**, 122001 (2002).
35. G. Blanpied *et al.*, Phys. Rev. Lett. **79**, 4337 (1997).
36. R. Beck *et al.*, Phys. Rev. **C 61**, 035204 (2000).
37. T. Sato and T.-S. H. Lee, Phys. Rev. **C63**, 055201 (2001); T.-S. H. Lee, this volume.
38. C. Alexandrou *et al.*, PoS Latt2005,091 (2006).
39. A. Tsapalis, Nucl. Phys. Proc. Suppl. **153**, 320 (2006).
40. V. Pascalutsa and M. Vanderhaeghen, Phys. Rev. Lett. **95**, 232001(2005) and this volume.
41. S. P. Wells, PAVI 2002, Mainz, Germany, June 5-8, 2002, and private communication.
42. C. Alexandrou, Th. Leontiou, J. W. Negele and A. Tsapalis, hep-lat/0607030.
43. S. L. Adler, Ann. Phys.(NY) **50**,189 (1968); Phys. Rev. **D 12**, 2644 (1975).
44. C. H. Llewellyn Smith, Phys. Rep. **3C**, 261 (1972).
45. V. Gimenez, L. Guitsit, F. Rapuano and M. Talevi, Nucl. Phys. **B531** 429 (1998).
46. D. Becirevic *et al.*, Nucl. Phys. **B734** (2006) 138.
47. N. Fettes and U. G. Meissner, Nucl. Phys. **A679**, 629 (2001).
48. N. C. Mukhopadhyay *et al.*, Nucl. Phys. **A633**, 481 (1998).